Supplementary Material and Figures to

Structure of the full human RXR/VDR nuclear receptor heterodimer complex with its DR3 target DNA

Igor Orlov[1], Natacha Rochel[1], Dino Moras[1], Bruno P. Klaholz[1]*

[1] IGBMC (Institute of Genetics and of Molecular and Cellular Biology), Department of Integrative Structural Biology, Centre National de la Recherche Scientifique (CNRS) UMR 7104 / Institut National de la Santé de la Recherche Médicale (INSERM) U964 / Université de Strasbourg, 1 rue Laurent Fries, 67404 Illkirch, France.

***To whom correspondence should be addressed. klaholz@igbmc.fr, Tel. ++33 388655755; FAX ++33 388653276**

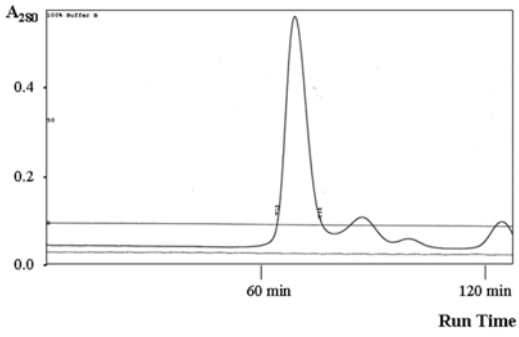

gel filtration profile

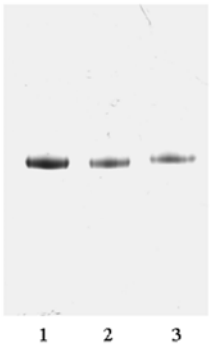

native gel

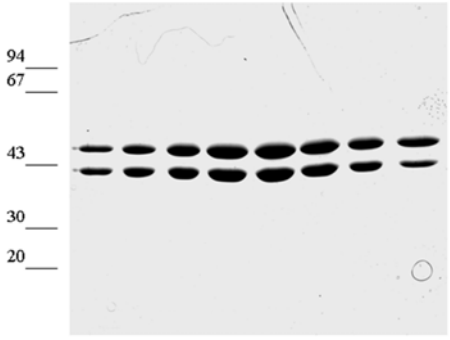

SDS gel

Characterization of the RXR/VDR/DR3 complex by size-exclusion chromatography (top), and by native (middle) and denaturing (bottom) gel electrophoresis.

Suppl. Fig. 1

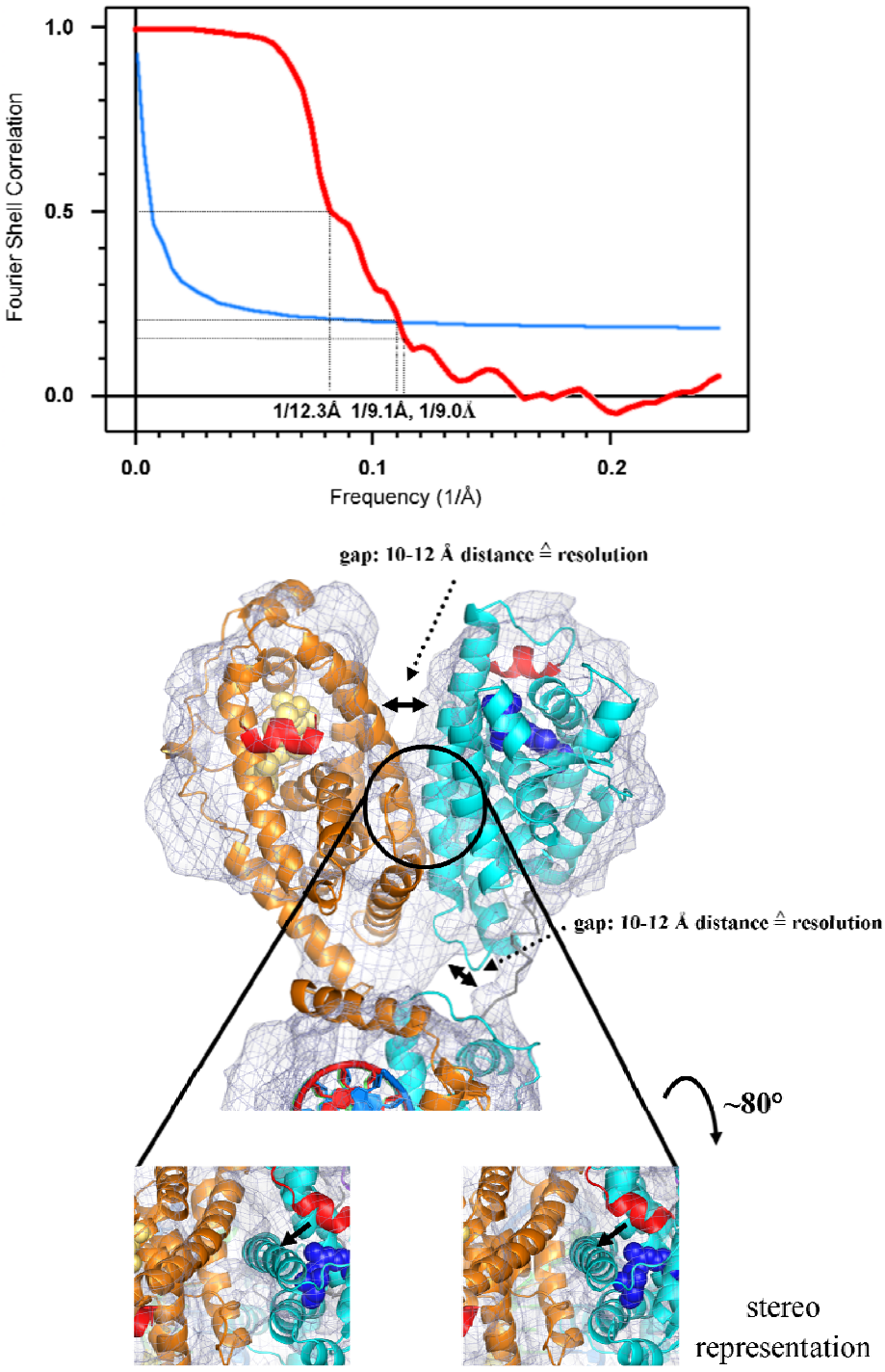

Resolution assessment according to the Fourier shell correlation (top) and to the features resolved in the map (bottom, RXR helix H10 is indicated).

Suppl. Fig. 2

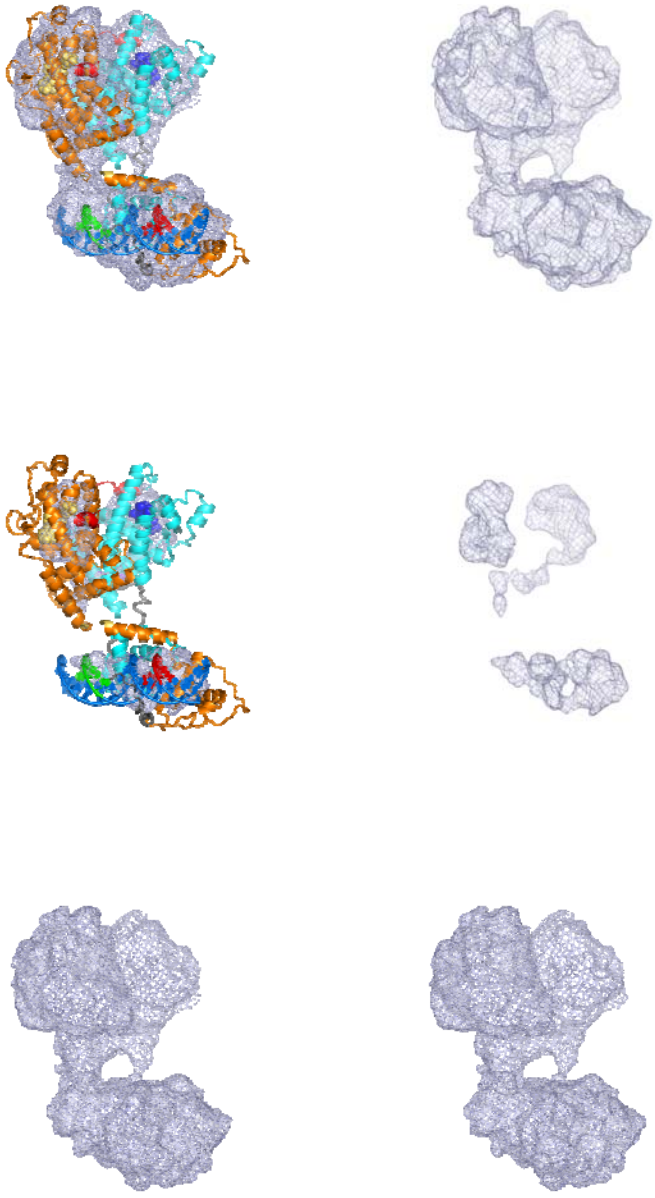

The cryo-EM map of the RXR/VDR/DR3 complex displayed at different contour levels (displayed with and without the fitted model) reveals a stronger density for the DNA (because of the phosphorus of the nucleotides) and some residual density for the core part of the LBD domains. Bottom: stereo representation of the raw cryo-EM map.

Suppl. Fig. 3

	Map Orientation	*DNA Polarity*	*LBD's Position*	*Cross Correlation*
1	Direct	Correct	Correct	0,832
2	Direct	Correct	Flipped	0,823
3	Direct	Flipped	Correct	0,828
4	Direct	Flipped	Flipped	0,823
5	Mirrored	Correct	Correct	0,826
6	Mirrored	Correct	Flipped	0,812
7	Mirrored	Flipped	Correct	0,810
8	Mirrored	Flipped	Flipped	0,810

Cross correlation (CC) coefficients for different fitting possibilities of the LBDs (as a heterodimer unit) and the DNA/DBDs; flipping of the LBDs inverses the RXR and VDR positions around the pseudo two-fold axis (main **Fig. 2C**), while flipping the DNA/DBDs inverts the polarity of the DNA. “Correct” is the orientation corresponding to the correct solution, and also represents the solution that is compatible with the connectivity constraint through the hinge region between LBDs and DBDs (specifically, solution 3 would not allow connecting the domains for distance reasons). The comparison of CC values confirms the unambiguous assignment of the components and also the handedness of the complex.

Suppl. Fig. 4

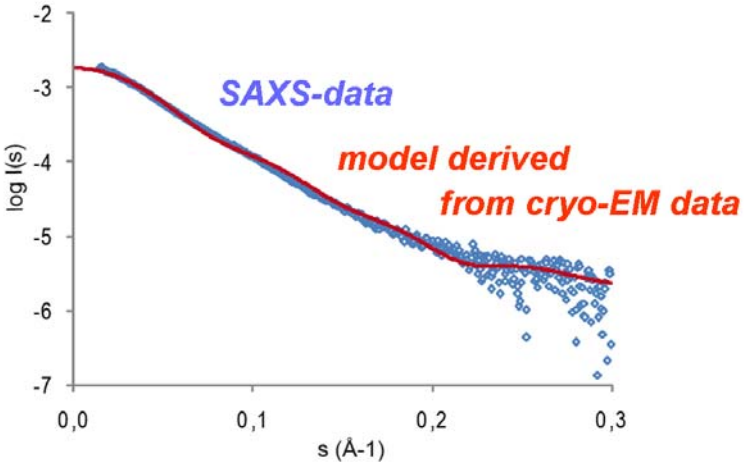

Comparison of the small angle X-ray diffraction (SAXS) curve of the RXR/VDR/DR3 complex in solution (measurements are represented as blue dots) with the theoretical curve (red) calculated from the model that was derived from the cryo-EM map. The global arrangement and conformation is rather similar, as is illustrated by the good correspondence at lower and medium s values (describing low and medium resolution components such as size and overall conformation and structure, the most prominent parameter being the radius of gyration).

Suppl. Fig. 5

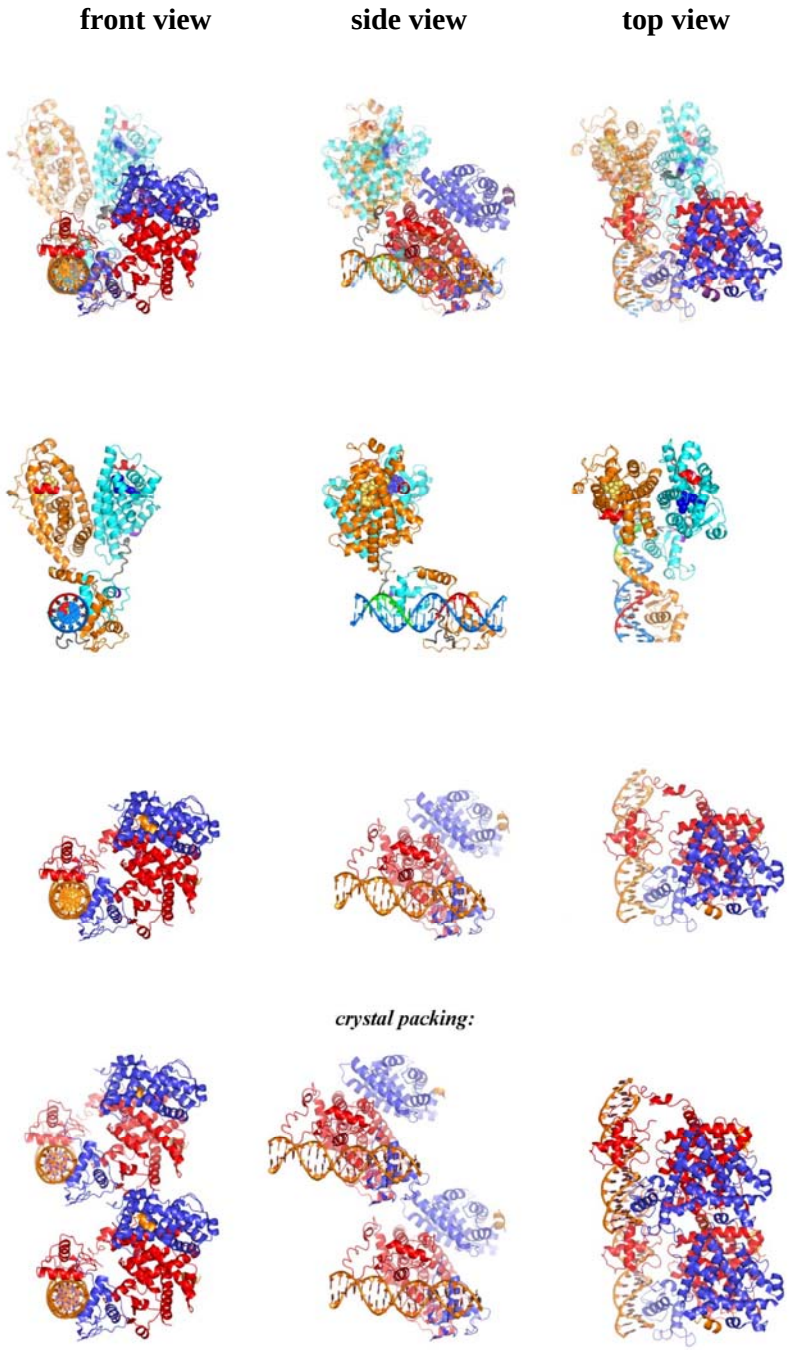

Comparison of the RXR/VDR/DR3 cryo-EM structure (this study) with that of the PPAR/RXR/DR1 crystal structure (Chandra *et al.*, 2008); coloring as in main **Fig. 1, 2&3**.

Suppl. Fig. 6

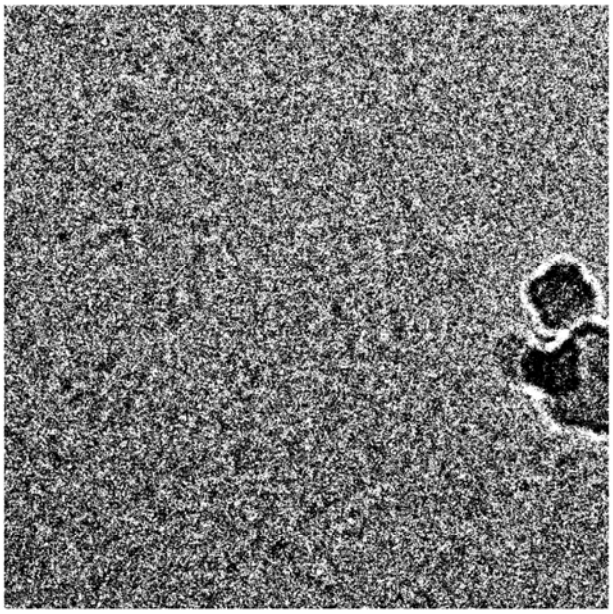

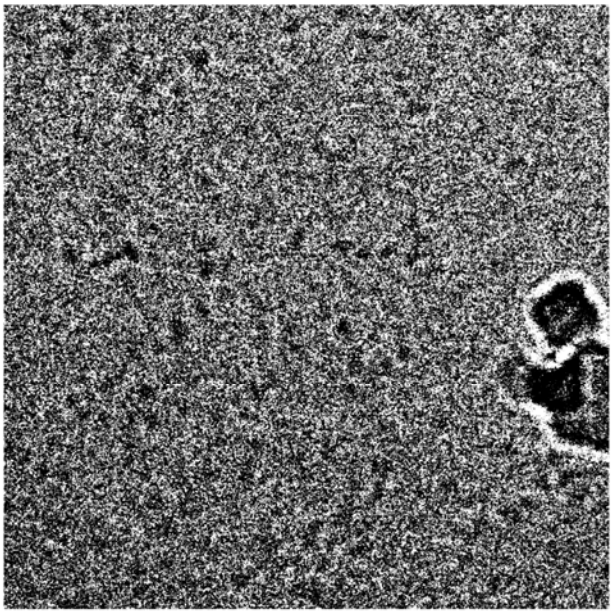

RXR/VDR/DR3 single particle cryo-EM images at different defocus values (defocus pairs); the second image recorded at higher defocus was used for particle selection only.

[Defocus is the amount of underfocus (when the focal point of the beam is after the specimen) applied when acquiring images with the electron microscope in order to improve the contrast while keeping as much of the high resolution information as possible.]

Suppl. Fig. 7

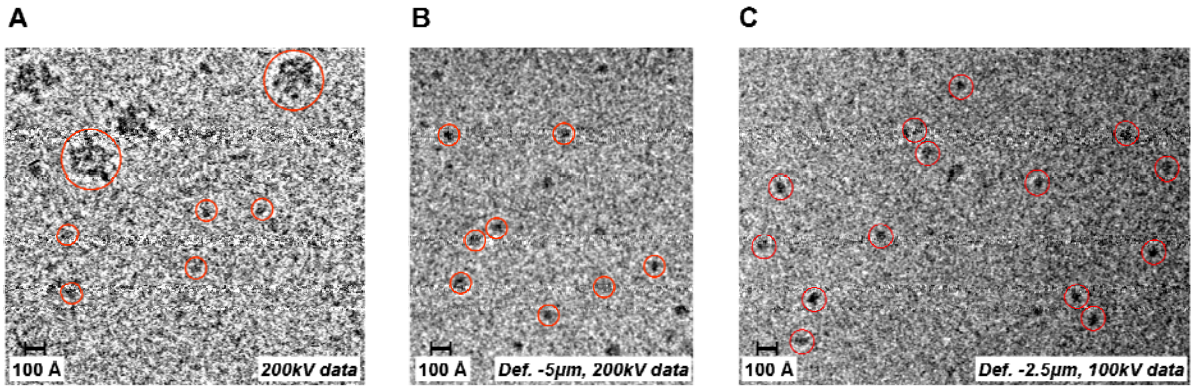

A CCD image of a flash-frozen hydrated sample containing the purified nuclear receptor mixed with 50S ribosomal subunits for comparison; scale bar is 100 Å; recorded on a transmission electron microscope (see Methods section) under cryo conditions at a defocus of ~3 µm at 200kV. Some particles are marked with red circles (the 100kDa NR particles are ~100 Å in size, while the ~1.5MDa 50S particles are up to ~220 Å in size).

B CCD image of a flash-frozen hydrated nuclear receptor sample after screening for optimal ice quality and particle distribution; recorded at a defocus of ~5 µm at 200kV.

C CCD image of the nuclear receptor complex sample, recorded at a defocus of ~2.5 µm at 100kV. The higher contrast obtained at 100kV allows to record images closer to focus (compared to ~5 µm at 200kV in panel **B**) while keeping a good contrast required for the further processing of the data. A larger, zoomed field of particles can be found in **Suppl. Fig. 9**.

Suppl. Fig. 8

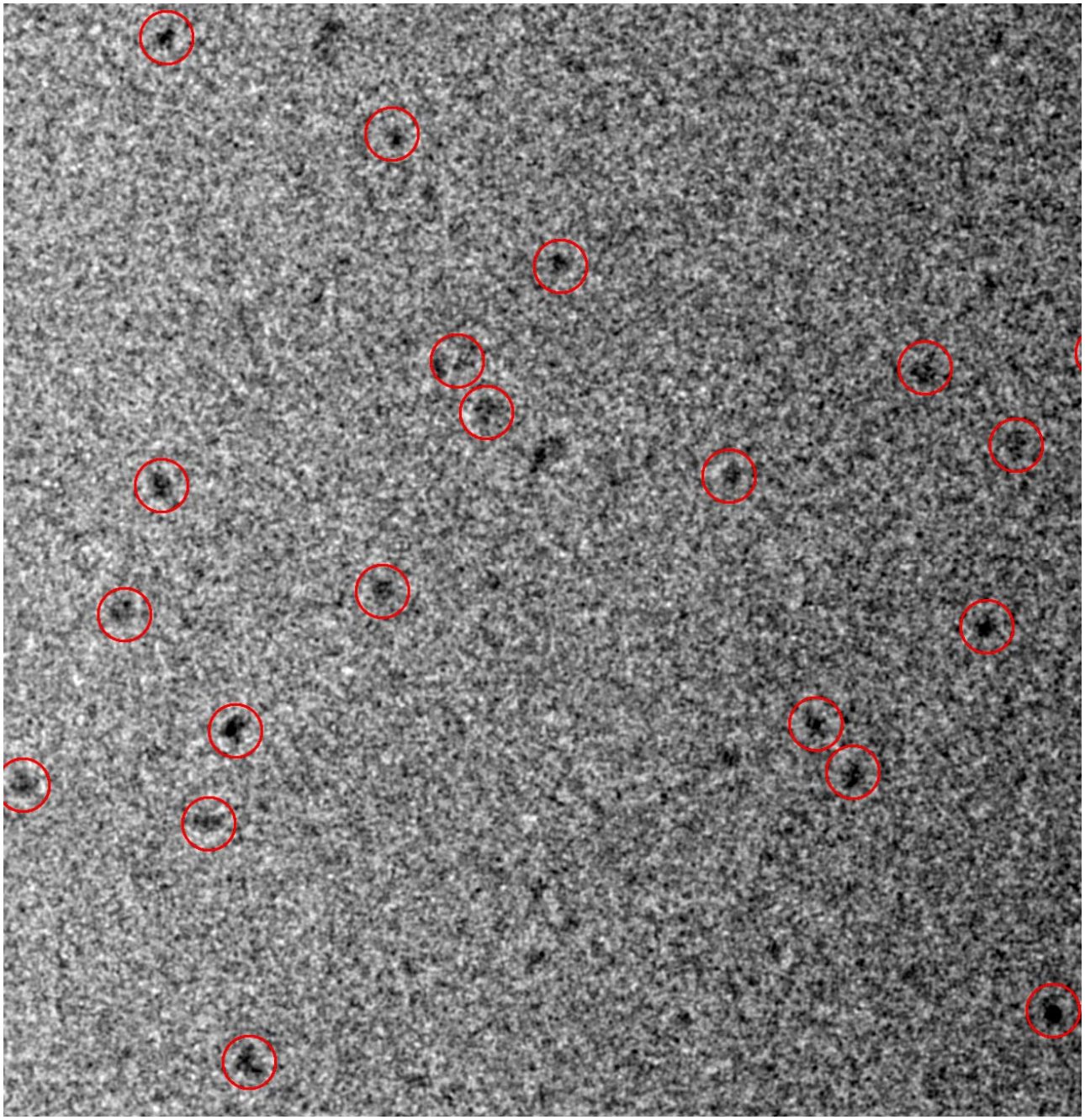

Zoomed version of **Suppl. Fig. 8C**. Cryo-EM image recorded at 100kV, defocus -2.5 µm (for comparison see **Fig. 1A** and **Suppl. Fig. 8B** where the image was recorded at 200kV and -5.0 µm defocus). The higher contrast obtained at an acceleration voltage of 100kV has also the advantage that images closer to focus can be recorded.

Suppl. Fig. 9

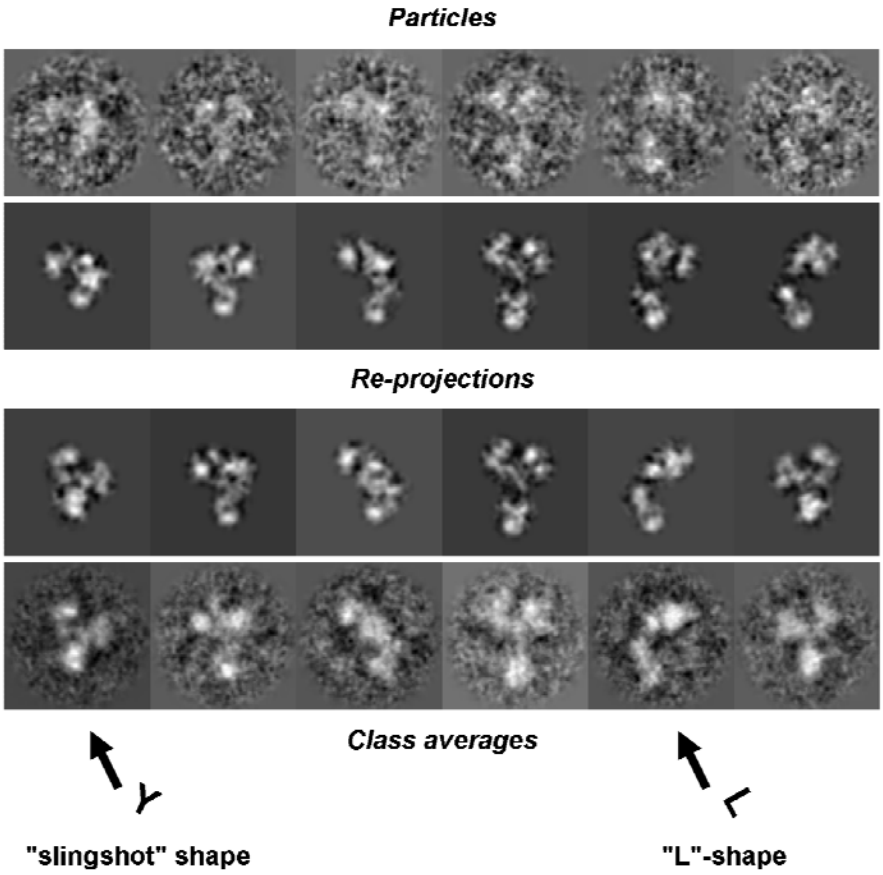

Comparison of raw particle images (first lane) with re-projections of the obtained 3D structure (second lane), and comparison of class averages (third lane, obtained by multivariate statistical analysis and classification using the 200kV data) with the corresponding re-projections of the three-dimensional reconstruction (fourth lane). The characteristic “L”- and “slingshot” shapes can be recognized in the class averages (compare these views with the side and front views in **Fig. 2A** and **B**).

Suppl. Fig. 10

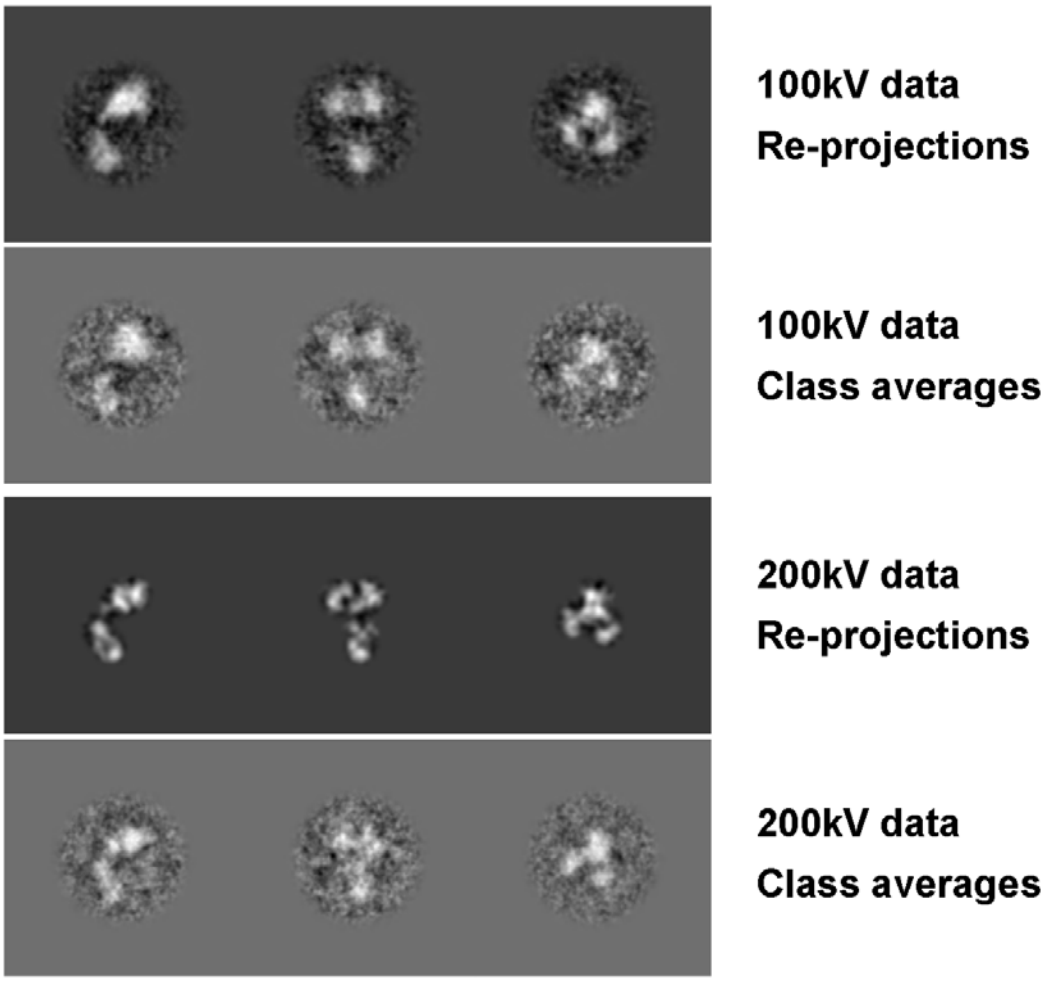

Class averages and corresponding orthogonal re-projections obtained for two independently determined *ab initio* structures using either 100kV or 200kV data. The two structures are very similar and fully consistent with each other (cross correlation coefficient is 0.87) and with the corresponding input class averages. These data provide important evidence, through the usage of a lower high tension on the electron microscope field emission gun unit, for the reliability of the final structure and thus validate the usage of cryo-EM for this relatively small macromolecular complex.

Suppl. Fig. 11

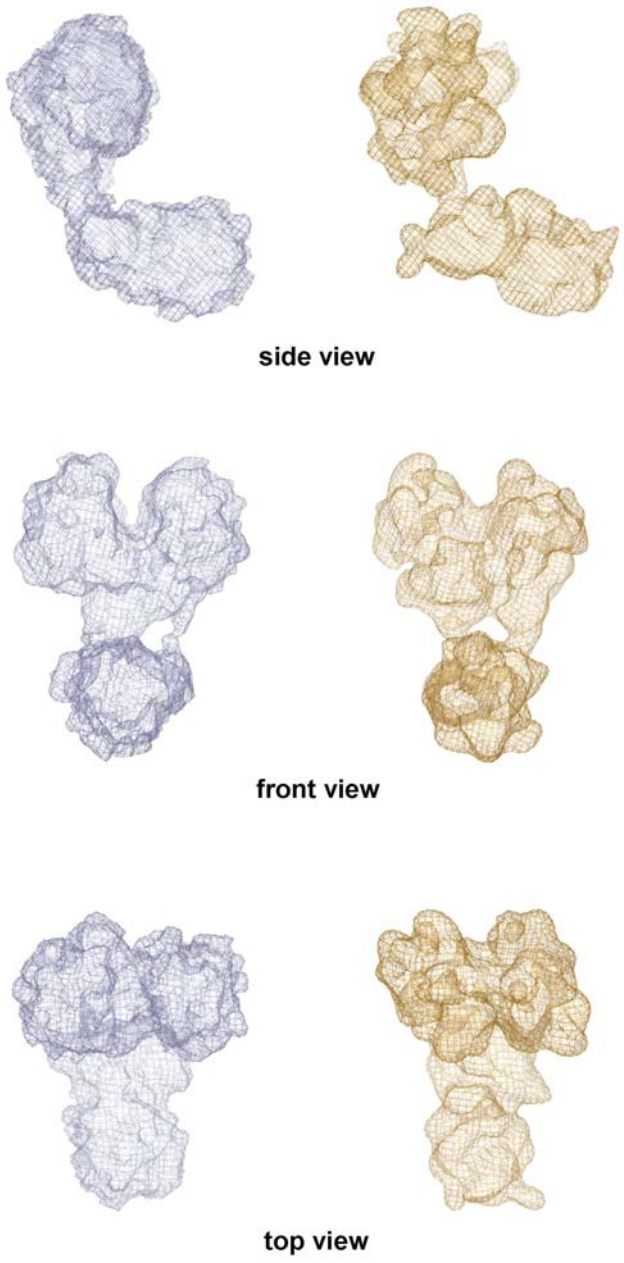

Maps calculated from the fitted model (orange, right; filtered to 12 Å resolution) in comparison with the experimental cryo-EM map (i.e. the raw reconstruction without docked crystal structures of the individual domains; blue, left).

Suppl. Fig. 12

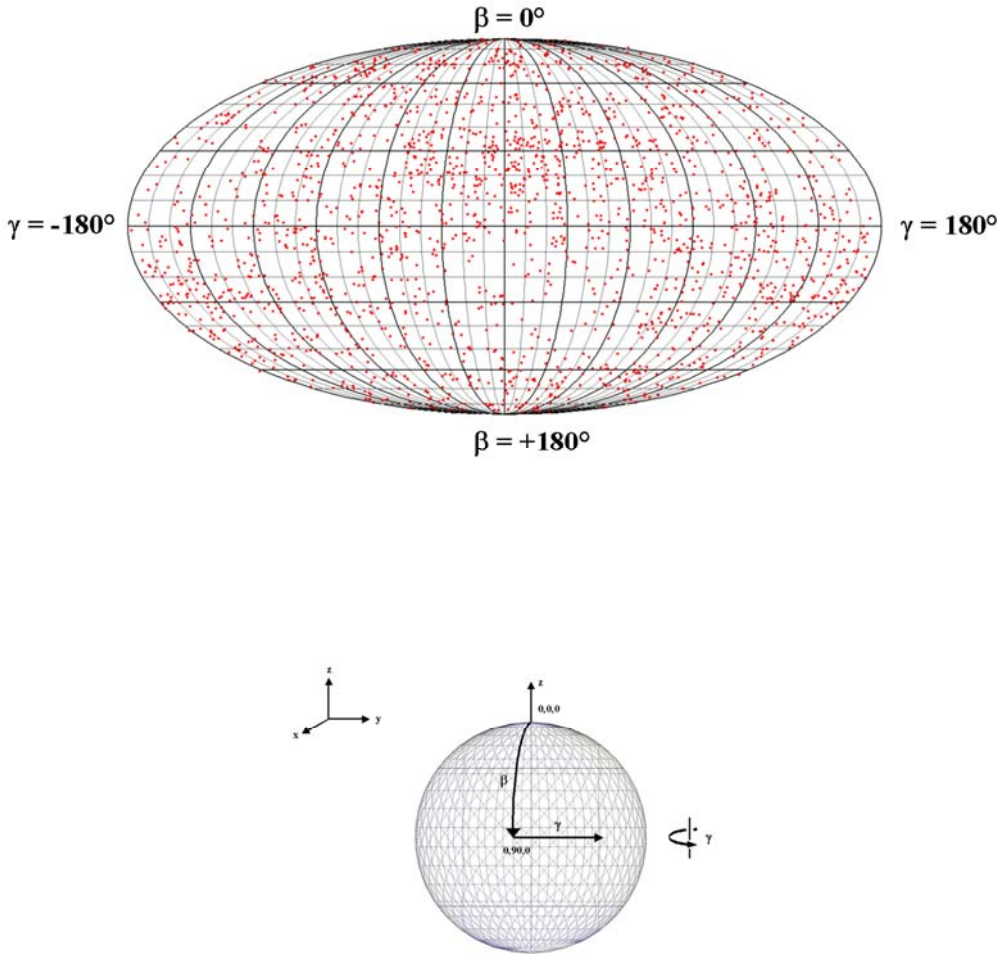

Angular distribution of particle views revealing a rather equal distribution; values indicate the β and γ Euler angles as defined on the sphere (bottom).

Suppl. Fig. 13